SCIENTIFIC CULTURE
www.sci-cult.com

SCIENTIFIC CULTURE, Vol. 12, No. 4, (2026), pp. 8224-8238
Open Access. Online & Print

DOI: 10.5281/zenodo.20720851

EXPERIMENTAL EVALUATION OF SEISMIC STRENGTHENING TECHNIQUES FOR ADOBE MASONRY STRUCTURES USING SHAKE TABLE AND IMPACT HAMMER TESTING

Chintan D. Patel [1*], Tarak Vora[2]

[1]Research Scholar, Department of Civil Engineering, Marwadi University, Rajkot, Gujarat, India*
[2] Professor, Department of Civil Engineering,Marwadi University, Rajkot, Gujarat, India

Received: 07/10/2025
Accepted: 07/02/2026

Corresponding Author: Chintan D. Patel

ABSTRACT

Non-engineered adobe masonry structures constitute a significant portion of the building stock in developing regions and are highly susceptible to earthquake-induced damage due to their low tensile strength, poor structural continuity, and lack of confinement. While several strengthening approaches have been proposed, limited experimental studies have systematically compared the effectiveness of different reinforcement materials under identical dynamic loading conditions. This study presents a comparative experimental investigation of seismic strengthening techniques for adobe masonry structures using reduced-scale (1:5) models subjected to shake table excitation. A total of seven models were constructed, comprising one unreinforced reference model and six strengthened configurations employing cold-formed steel, geogrid, and hemp fibre reinforcement. Material properties were established through standard geotechnical and compressive strength tests. Dynamic characteristics, including natural time period and damping, were obtained from impact hammer testing, and seismic response was evaluated through shake table testing within a frequency range of 0–25 Hz. The seismic performance of the models was quantified using capacity curves expressed in terms of base shear coefficient versus drift ratio. The results demonstrate that strengthening significantly alters the post-elastic response of adobe masonry. Geogrid reinforcement exhibited the highest lateral load capacity, achieving a maximum base shear coefficient of 5.284, corresponding to an increase of approximately 150–180% over the unreinforced model. Cold-formed steel reinforcement resulted in the highest damping enhancement (up to ~200%), indicating improved energy dissipation, while hemp fibre reinforcement provided enhanced deformation capacity and ductile behavior. The findings highlight that confinement-based strengthening mechanisms play a critical role in improving seismic performance by delaying crack propagation and enabling stress redistribution. The study provides experimental evidence supporting the use of low-cost reinforcement strategies for enhancing the seismic resilience of adobe masonry structures.

KEYWORDS: Vernacular Structures, adobe masonry; seismic performance; seismic strengthening; shake table testing; geogrid reinforcement; cold-formed steel; hemp fibre; ductility; energy dissipation; capacity curve.

Copyright: © 2026. This is an open-access article distributed under the terms of the Creative Commons Attribution License. (https://cre-ativecommons.org/licenses/by/4.0/).

1. INTRODUCTION

Vernacular adobe structures represent traditional construction systems developed using locally available materials and indigenous construction techniques that have evolved over generations. These structures constitute a significant portion of the building stock in developing countries and are generally classified as non-engineered buildings due to the absence of formal design and construction practices (Ikuga and Murray 2012; Arya et al. 2013). As a result, they exhibit high vulnerability to seismic hazards, primarily due to inadequate structural continuity, poor material quality, and lack of reinforcement (Lagomarsino and Giovinazzi 2006; Lourenço 2006).

Adobe, typically composed of clay, sand, water, and organic fibres such as straw, offers several advantages, including low cost, thermal efficiency, and environmental sustainability (Minke 2006). However, its inherent brittleness and low tensile strength result in poor resistance to lateral loads, making adobe masonry highly susceptible to cracking and sudden collapse under earthquake excitation (Silveira et al. 2012; Griffith et al. 2003). Post-earthquake field investigations consistently indicate that unreinforced masonry and adobe structures are among the most severely damaged structural systems.

Extensive research has demonstrated that the seismic performance of masonry structures can be significantly improved through the incorporation of simple earthquake-resistant features such as horizontal bands, vertical reinforcement, and improved wall-to-wall and wall-to-roof connections (Paulay and Priestley 1992; Tomazevic 1999; Bothara and Brzev 2011). More recent studies have explored advanced strengthening techniques, including fibre-based reinforcement, geosynthetics, and metallic systems, to enhance the structural response of masonry systems under seismic loading (Kafodya et al. 2019; Tipler et al. 2010; Behera et al. 2022; Ye et al. 2018). These studies have shown that confinement-based and tensile reinforcement mechanisms can significantly improve lateral load capacity, ductility, and energy dissipation.

Shake table testing has emerged as a reliable experimental approach for evaluating the dynamic response and failure mechanisms of masonry structures under simulated earthquake excitation. Such studies enable direct observation of crack initiation, propagation, and collapse behaviour under controlled conditions, thereby providing insights beyond analytical modelling (ElGawady et al. 2004; Degli Abbati et al. 2023; Kaya et al. 2024). Due to practical constraints associated with full-scale testing, reduced-scale modelling is commonly adopted; however, appropriate similitude relationships must be maintained to ensure representative structural behaviour (Tolles and Krawinkler 1990).

Despite these advancements, there remains a lack of systematic experimental studies that directly compare the effectiveness of different strengthening materials for adobe masonry structures under identical loading and boundary conditions. In particular, comparative assessments of metallic, geosynthetic, and natural fibre-based reinforcement systems within a unified experimental framework are limited in the existing literature.

In this context, the present study aims to experimentally evaluate and compare the effectiveness of three distinct seismic strengthening techniques—cold-formed steel, geogrid reinforcement, and hemp fibre rope—using shake table testing of reduced-scale (1:5) adobe masonry models. A total of seven models, including one unreinforced reference model and six strengthened configurations, were constructed and tested under controlled dynamic excitation. The study focuses on quantifying the influence of these strengthening techniques on dynamic characteristics, lateral load capacity, ductility, and failure mechanisms, thereby providing practical insights for improving the seismic resilience of non-engineered adobe structures.

2. MODEL GEOMETRY AND SIMILITUDE

A total of seven reduced-scale adobe masonry models were constructed at a geometric scale of 1:5 to experimentally investigate the influence of different seismic strengthening techniques. All models were designed with identical plan dimensions, wall thickness, opening configurations, and construction details to ensure that the observed variations in response could be attributed solely to the strengthening interventions. The plan configuration of the prototype structure, adopted as the reference for scaling, is shown in Fig. 1.

The geometric properties of adobe bricks used in the prototype and corresponding reduced-scale models are presented in Table 1.

Table 1 Geometric properties of adobe bricks used in prototype and reduced-scale models

Brick type	Scale	Length, L (mm)	Breadth, B (mm)	Height, H (mm)
Prototype adobe brick	1:1	250	300	90
Reduced-scale adobe brick	1:5	50	60	18

The dimensions of the reduced-scale bricks were obtained using the adopted geometric scale factor of 1:5, thereby ensuring geometric similitude between the prototype and model structures.

Reduced-scale modelling is a widely accepted approach in experimental earthquake engineering, particularly for masonry systems, where full-scale testing is often impractical due to limitations in laboratory capacity, actuator constraints, and economic considerations. However, the validity of reduced-scale experiments depends on the ability to preserve the governing physical relationships between the model and the prototype through appropriate similitude conditions (Tolles and Krawinkler 1990; ElGawady et al. 2004).

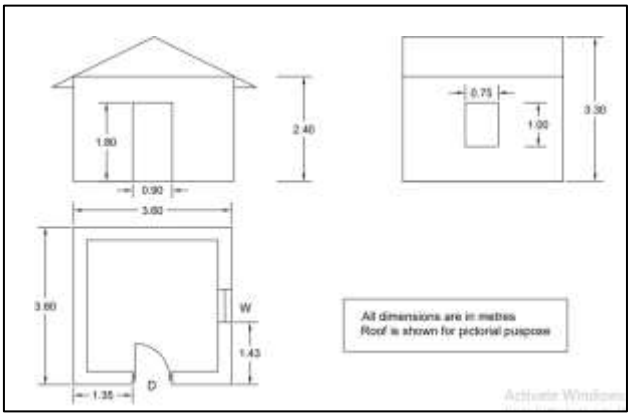

Fig 1 Plan of Structure

2.1 Similitude Considerations

The dynamic response of masonry structures under seismic loading is governed by the equation of motion:

$$M\ddot{u} + Cu + Ku = F(t)$$

Where, M, C, and K represent mass, damping, and stiffness matrices, respectively. To ensure that the reduced-scale models reproduce the essential characteristics of the prototype response, geometric, kinematic, and dynamic similitude must be satisfied such that the relative proportions of inertia, stiffness, and damping forces are maintained.

In the present study, a geometric scale factor of $\lambda=5$ was adopted. Based on similitude theory, the corresponding scaling relationships for key physical parameters were defined as follows: the frequency scales as $f_p = (f_m/\lambda)$, the time period as $t_p = (t_m/\lambda)$, the displacement as $\delta_p = (\lambda\ \delta_m)$, the force as $F_p = (\lambda^2 F_m)$, and the acceleration as $a_p = (a_m/\lambda)$.

Where the subscripts p and m denote the prototype and model, respectively.

These relationships are consistent with classical scaling laws for structural dynamics, where force scales with the square of the geometric factor and displacement scales linearly. The scaling of time and frequency ensures that the dynamic characteristics, including natural periods and mode shapes, are appropriately represented in the model system (Tolles and Krawinkler 1990).

2.2 Assumptions and Limitations of Similitude

Exact similitude in masonry structures is inherently difficult to achieve due to the heterogeneous and nonlinear nature of adobe material, as well as scale-dependent effects such as cracking, bond behavior, and energy dissipation mechanisms. In particular, parameters such as damping and fracture characteristics cannot be perfectly scaled, as they are influenced by microstructural properties and construction variability.

In the present study, the following assumptions were adopted:

a) Material properties (density and stress–strain characteristics) were assumed to be scale-independent.
b) Gravitational stresses were neglected, as inertial forces dominate the response under dynamic excitation for single-storey structures.
c) Boundary conditions and construction techniques were maintained consistent across all models.

These assumptions are consistent with established experimental practices for reduced-scale masonry testing (ElGawady et al. 2004; Degli Abbati et al. 2023).

2.3 Justification for Experimental Approach

The primary objective of this investigation is to perform a comparative evaluation of strengthening techniques rather than to replicate the exact prototype response. Therefore, maintaining internal consistency across all models is more critical than achieving strict similitude in absolute terms.

Since all seven models were constructed using identical materials, geometric proportions, and loading protocols, the experimental framework ensures that differences in seismic performance—such as variations in lateral strength, ductility, damping, and failure modes—are directly attributable to the strengthening techniques employed.

Furthermore, previous shake table studies on masonry systems have demonstrated that reduced-scale models, when properly designed, are capable of capturing essential behavioural characteristics such as crack initiation, propagation patterns, and collapse mechanisms (ElGawady et al. 2004; Degli Abbati et

al. 2023). The present methodology therefore provides a reliable basis for evaluating the relative effectiveness of different seismic strengthening strategies for adobe masonry structures.

3. MATERIAL PROPERTIES

3.1 Physical and Mechanical Characterization of Adobe

The seismic performance of adobe masonry structures is strongly governed by the physical and mechanical properties of the constituent material, particularly density, moisture characteristics, compressive strength, and tensile (flexural) strength. Due to the inherent variability of earthen materials, a systematic material characterization program was undertaken to establish an appropriate mix composition and to ensure consistency across all experimental models.

3.1.1 Mix Selection and Soil Classification

Three trial mixes with varying clay-to-sand proportions (60:40, 50:50, and 40:60 by weight) were prepared and evaluated based on workability, shrinkage behavior, and mechanical performance. The results of this evaluation are summarized in Table 2.Three trial mixes with varying clay-to-sand proportions (60:40, 50:50, and 40:60 by weight) were prepared and evaluated, as summarized in Table 2. The evaluation was carried out based on workability, shrinkage behavior, and mechanical strength characteristics. Among these, the 60:40 mix (M1) was selected for further use, as it exhibited minimal shrinkage cracking and provided adequate cohesion and workability. This observation is consistent with previous studies indicating that higher clay content improves binding characteristics, while excessive sand content reduces cohesion and leads to brittle behaviour (Minke 2006; Silveira et al. 2012).

Table 2 Mix proportions and Material Properties of Adobe Specimens

Mix ID	Clay (%)	Sand (%)	MDD (g/cm³)	OMC (%)	Compressive Strength (MPa)	Flexural Strength (MPa)	Remarks
M1	60	40	1.71	16.0	3.14	2.90	Selected mix
M2	50	50	1.68	15.48	2.45	1.85	Moderate cracking
M3	40	60	1.62	14.93	1.72	1.10	Brittle behavior

Among the three mixes, the 60:40 proportion (M1) exhibited minimal shrinkage cracking, adequate cohesion, and superior strength characteristics, and was therefore selected for the preparation of all experimental specimens. This observation is consistent with previous studies, which indicate that higher clay content improves bonding characteristics, while excessive sand content reduces cohesion and leads to brittle behaviour (Minke 2006; Silveira et al. 2012).

The soil used for adobe preparation was classified as CH-type (high plasticity clay) based on standard geotechnical classification procedures. Such soils provide good cohesion for block formation but require careful control of moisture content to minimize shrinkage effects.

3.1.2 Compaction Characteristics

Compaction tests were conducted to determine the maximum dry density (MDD) and optimum moisture content (OMC) of the selected adobe mix. The MDD and OMC were found to be 1.71 g/cm^3 and 16%, respectively.

These parameters were used to control the preparation of adobe blocks to ensure uniform density and consistent mechanical performance across all specimens. The relatively high dry density achieved indicates effective compaction and a low void ratio, which contributes to improved stiffness and strength of the adobe material.

Moisture content plays a critical role in adobe preparation, as excess water leads to increased porosity and reduced strength, whereas insufficient moisture results in inadequate bonding between soil particles. Proper control of these parameters is therefore essential for achieving reliable and reproducible material properties (Silveira et al. 2012).

3.1.3 Compressive Strength

The compressive strength of adobe specimens was determined through unconfined compression tests. The experimental setup used for testing is shown in Fig. 2.

Fig 2 Experimental setup for unconfined compression testing of adobe specimens

The results of compressive strength testing are summarized in Table 3.

Table 3. Compressive strength of adobe specimens

Specimen	Length (mm)	Width (mm)	Height (mm)	Peak Load (kN)	Compressive Strength (MPa)
S1	129.6	134.4	133.1	53.5	3.07
S2	137.7	139.7	140.8	71.5	3.72
S3	136.65	140.8	134.4	50.5	2.62
Average Compressive Strength					**3.14**

The average compressive strength obtained was 3.14 MPa, which lies within the typical range reported for unstabilized adobe masonry and satisfies the minimum requirements specified in NZS 4298 (1998). The relatively high strength observed can be attributed to proper mix proportioning, effective compaction, and controlled curing conditions.

From a structural perspective, compressive strength governs the axial load-carrying capacity and contributes to the overall stiffness of masonry walls. However, under seismic loading, compressive strength alone does not ensure satisfactory performance, as adobe structures are primarily vulnerable due to their low tensile resistance and brittle failure characteristics (Lourenço 2006; Tomazevic 1999).

3.1.4 Flexural (Tensile) Strength

The tensile capacity of adobe was evaluated indirectly through flexural strength testing. A brick specimen of dimensions 250 mm × 300 mm × 80 mm was tested, and the flexural strength was found to be 2.9 MPa.

According to NZS 4298 (1998), the recommended minimum flexural strength for adobe materials is 0.25 MPa, indicating that the tested specimens significantly exceed the required threshold. This demonstrates adequate resistance to bending and crack initiation under lateral loading conditions.

Flexural strength is particularly important for seismic performance, as masonry walls subjected to earthquake loading experience bending and tensile stresses that lead to crack formation. Higher flexural strength contributes to improved crack resistance, delayed failure, and enhanced structural integrity.

The observed strength can be attributed to the balanced clay–sand ratio, which provides sufficient cohesion while maintaining dimensional stability. The clay fraction enhances bonding, whereas the sand fraction reduces shrinkage and improves overall material stability (Minke 2006; Kafodya et al. 2019).

3.1.5 Influence of Material Properties on Seismic Behaviour

The experimentally determined material properties have direct implications for the seismic response of adobe masonry structures. In particular:

Density and compaction influence mass and stiffness, thereby affecting natural frequency and inertia forces.

Compressive strength governs load-bearing capacity and resistance to crushing failure.

Flexural strength controls crack initiation and propagation under lateral loading.

Despite the relatively adequate compressive strength, adobe masonry remains highly vulnerable to seismic loading due to its low tensile strength and brittle failure behaviour, which can lead to sudden collapse once cracking initiates (Griffith et al. 2003; Silveira et al. 2012).

Therefore, strengthening techniques that enhance tensile resistance, confinement, and energy dissipation are essential to improve the seismic performance of adobe structures. The material properties obtained in this study serve as a baseline for evaluating the effectiveness of the strengthening systems investigated in subsequent sections.

3.1.6 Variability and Experimental Considerations

Adobe is a non-homogeneous material, and its properties are influenced by factors such as soil composition, mixing procedures, compaction effort, and curing conditions. As a result, variability in test results is expected.

To minimize variability, all specimens in this study were prepared using identical procedures and tested under controlled laboratory conditions. The reported values represent average results and are considered adequate for comparative evaluation.

Previous studies have emphasized the importance of standardized testing and careful specimen preparation to obtain reliable mechanical properties of adobe materials (Silveira et al. 2012). The methodology adopted in this study is consistent with established experimental practices.

3.2 Strengthening Materials and Configuration

In order to enhance the seismic performance of adobe masonry structures, three distinct strengthening systems—cold-formed steel, geogrid reinforcement, and hemp fibre rope—were investigated in this study. These systems were selected to represent different reinforcement mechanisms, namely metallic confinement, polymer-

based confinement, and natural fibre-based reinforcement. The selection was guided by considerations of structural effectiveness, constructability, cost, and suitability for application in non-engineered construction.

All strengthening systems were applied to the reduced-scale models in controlled configurations to enable a direct comparison of their influence on dynamic characteristics, lateral load capacity, ductility, and failure mechanisms.

3.2.1 Cold-Formed Steel Reinforcement

Cold-formed steel (CFS) sections were used as an external strengthening system to improve the structural integrity and lateral resistance of adobe masonry walls. The reinforcement was provided in both localized and grid-type configurations to investigate the effect of reinforcement distribution on seismic performance.

The primary contribution of cold-formed steel lies in its high tensile strength and ductile behaviour, which enables it to resist tensile stresses that are otherwise not sustained by adobe material. Under seismic loading, the steel elements act as crack arrestors by bridging developing cracks and limiting their propagation. This results in improved stiffness retention and delayed onset of structural degradation.

In addition, the presence of steel reinforcement enhances energy dissipation through hysteretic behaviour during cyclic loading. This is reflected in increased damping characteristics observed in reinforced models. However, the effectiveness of cold-formed steel reinforcement in adobe systems is strongly influenced by the quality of interaction between the steel elements and the surrounding earthen matrix. Due to the relatively weak bond and low stiffness of adobe, full composite action is not always achieved, which may limit the utilization of the tensile capacity of steel (Ye et al. 2018; Reyes et al. 2012).

Despite these limitations, cold-formed steel remains a practical strengthening solution due to its ease of installation, availability, and ability to significantly enhance post-cracking behaviour.

3.2.2 Geogrid Reinforcement

Geogrid reinforcement was employed as a confinement-based strengthening technique to improve the in-plane shear resistance and overall stability of adobe masonry walls. The geogrid used in this study (CTMGGU 100/30) possesses high tensile strength in orthogonal directions, enabling it to effectively resist tensile forces induced during seismic excitation.

The strengthening mechanism of geogrid reinforcement is primarily governed by its ability to provide lateral confinement and promote stress redistribution within the masonry. When subjected to lateral loading, the geogrid interacts with the adobe matrix through mechanical interlocking and frictional resistance, resulting in improved load transfer and enhanced structural integrity.

This confinement effect delays crack initiation and controls crack propagation, thereby increasing both the strength and ductility of the system. Furthermore, geogrid reinforcement contributes to improved post-peak behaviour by preventing sudden brittle failure and enabling gradual degradation of stiffness.

Two configurations were considered in this study: surface-mounted reinforcement and bed-joint reinforcement. Surface application provides global confinement to the wall, while bed-joint reinforcement improves interlayer bonding and enhances resistance to shear sliding. Previous experimental studies have demonstrated that geogrid-reinforced masonry exhibits significant improvements in lateral strength, deformation capacity, and energy dissipation (Tipler et al. 2010; Behera et al. 2022).

3.2.3 Hemp Fibre Reinforcement

Hemp fibre rope was used as a natural reinforcement material to enhance the ductility and deformation capacity of adobe masonry. Natural fibres are increasingly being explored as sustainable alternatives to synthetic reinforcement due to their low cost, biodegradability, and compatibility with earthen materials.

The reinforcing action of hemp fibre is primarily associated with crack bridging and tensile resistance. As cracks initiate and propagate within the adobe matrix, the fibres provide resistance by transferring tensile stresses across crack interfaces, thereby reducing crack width and delaying failure. Unlike rigid reinforcement systems, fibre-based reinforcement allows controlled deformation, resulting in improved ductile behaviour and enhanced energy absorption capacity.

However, the contribution of hemp fibre to strength enhancement is relatively limited compared to metallic or polymer-based reinforcement systems. Its effectiveness is influenced by factors such as fibre orientation, distribution, bonding characteristics, and moisture sensitivity. Despite these limitations, hemp fibre reinforcement offers a viable low-cost solution for improving seismic performance, particularly in

rural and resource-constrained environments (Kafodya et al. 2019; Sathiparan and Meguro 2015).

3.2.4 Comparative Mechanisms of Strengthening Systems

The three strengthening systems considered in this study differ significantly in their mode of action and influence on structural response.

Cold-formed steel primarily enhances tensile resistance and energy dissipation, resulting in improved damping behaviour.

Geogrid reinforcement provides confinement and stress redistribution, leading to increased lateral strength and controlled crack propagation.

Hemp fibre reinforcement improves ductility and deformation capacity through crack bridging and flexible load transfer mechanisms.

4. EXPERIMENTAL PROGRAM AND MODEL CONSTRUCTION

This section presents the construction of reduced-scale adobe masonry models and the experimental procedures adopted to evaluate their dynamic and seismic performance. The experimental program consists of two stages: (i) construction of geometrically identical reduced-scale models with different strengthening configurations, and (ii) dynamic testing using impact hammer and shake table excitation.

A total of seven models were constructed at a geometric scale of 1:5, comprising one unreinforced reference model (U1) and six strengthened models incorporating cold-formed steel, geogrid, and hemp fibre reinforcement systems. All models were designed with identical plan dimensions, wall thickness, and layout, ensuring that variations in response could be attributed solely to the strengthening configurations.

4.1 Construction of Reduced-Scale Models

The reduced-scale adobe masonry models were constructed using the selected 60:40 clay–sand mix, as described in Section 3. The brick dimensions and overall geometry were scaled according to the similitude relationships discussed in Section 2, ensuring geometric consistency between prototype and model configurations.

A total of seven models—U1, A1, A2, B1, B2, C1, and C2—were constructed. All models had identical plan dimensions, wall thickness, and layout. The only distinguishing parameter among the models was the type and configuration of seismic strengthening system employed. This approach ensures that any observed variation in structural response is directly attributable to the strengthening technique.

4.2 Description of Model Configurations

Model U1 (Unreinforced Reference Model)

Model U1 represents a conventional adobe masonry structure without any strengthening provisions. It serves as the baseline model for comparison with all strengthened configurations.

The model was constructed using standard adobe masonry techniques, without any additional reinforcement or confinement mechanisms. Under seismic loading, such structures are expected to exhibit brittle behaviour characterized by early crack initiation, rapid crack propagation, and sudden collapse due to the low tensile strength and poor structural continuity of adobe masonry (Griffith et al. 2003).

Model A1 (Cold-Formed Steel – Localized Reinforcement)

Model A1 incorporates cold-formed steel strips placed at critical stress concentration zones, including corners, around openings, and at lintel levels. These locations are typically vulnerable to stress concentration and crack initiation during seismic excitation.

The steel strips act as localized reinforcement elements that enhance tensile resistance and provide confinement at key regions. This results in improved crack control and delays the onset of structural damage. However, since reinforcement is limited to discrete locations, the global stiffness and load redistribution capacity of the structure remain relatively unchanged compared to more distributed reinforcement systems.

Model A2 (Cold-Formed Steel – Grid Reinforcement)

Model A2 utilizes cold-formed steel strips arranged in a grid pattern over the wall surface, providing distributed reinforcement throughout the structure. This configuration enhances both local and global structural behaviour.

The grid system improves stress redistribution and provides continuous tensile resistance across the wall surface. Under seismic loading, the steel grid acts as a crack-bridging mechanism, reducing crack widths and preventing sudden brittle failure. Additionally, the distributed nature of reinforcement enhances energy dissipation through hysteretic behaviour during cyclic loading (Ye et al. 2018).

However, the effectiveness of this system depends on the bond interaction between the steel strips and the adobe matrix, which may limit full composite action.

Model B1 (Geogrid – Surface Strengthening)

Model B1 was strengthened using a wall-surface geogrid reinforcement technique, which provides confinement to the adobe masonry.

In this configuration, polypropylene strips were embedded within the bed joints during construction. After the completion of the masonry, the geogrid was attached both internally and externally using these embedded strips. This method ensures proper anchorage and load transfer between the geogrid and the adobe matrix.

Surface strengthening is widely used due to its ease of application and effectiveness in improving structural performance. The geogrid provides lateral confinement, enhances stress distribution, and delays crack initiation. As a result, the structure exhibits improved lateral load capacity and ductility under seismic loading (Tipler et al. 2010; Behera et al. 2022).

Model B2 (Geogrid – Bed-Joint Reinforcement)

Model B2 employs geogrid reinforcement placed within alternate bed joints of the masonry. This technique is used to overcome limitations associated with surface strengthening, such as poor bonding due to surface irregularities and susceptibility to environmental degradation.

In this model, geogrid strips were placed within the bed joints at regular intervals during construction. This configuration improves interlayer bonding and enhances resistance to shear sliding between masonry layers.

The bed-joint reinforcement mechanism contributes to improved structural integrity by increasing shear resistance and providing distributed tensile reinforcement within the masonry. It also reduces the likelihood of delamination and improves durability under environmental exposure.

Model C1 (Hemp Fibre – Surface Grid Reinforcement)

Model C1 incorporates hemp fibre ropes arranged in a grid pattern on the wall surface. The ropes were connected using horizontally placed strands to form a continuous reinforcement network.

This configuration provides confinement and tensile resistance through a flexible reinforcement system. The hemp fibres act as crack-bridging elements, allowing controlled deformation and enhancing ductility. Unlike rigid reinforcement systems, the flexibility of hemp fibres enables energy absorption and reduces stress concentration within the structure.

The grid arrangement ensures uniform distribution of reinforcement, improving overall structural performance under seismic loading.

Model C2 (Hemp Fibre – Junction Reinforcement)

Model C2 utilizes hemp fibre ropes specifically at critical locations such as wall junctions and around openings. These regions are highly susceptible to stress concentration and structural failure during seismic events.

By reinforcing these critical zones, the system improves load transfer between intersecting walls and enhances structural continuity. During testing, the reinforced junctions tend to behave as a single unit, reducing the likelihood of localized failure.

This targeted reinforcement approach is particularly effective in improving the integrity of connections, which are often the weakest points in adobe masonry structures.

Fig 3 Model U1

Fig 4 Model A1

Fig 5 Model A2

Fig 6 Model B1

Fig 7 Model B2

Fig 8 Model C1

Fig 9 Model C2

The strengthening configurations adopted in this study represent different reinforcement mechanisms, including localized strengthening, distributed confinement, and tensile reinforcement, enabling a systematic comparison of their influence on seismic response

4.3 Experimental Testing Program

The dynamic performance of the constructed adobe masonry models was evaluated through a combination of impact hammer testing and shake table testing. These two experimental approaches were selected to capture both the linear dynamic characteristics and the nonlinear seismic response of the models.

Impact hammer testing was conducted to determine the fundamental dynamic properties of the structures, including natural time period and damping ratio. Shake table testing was subsequently performed to evaluate the response of the models under controlled dynamic excitation, including damage progression, failure mechanisms, and load–deformation behaviour.

Such combined experimental approaches are widely adopted in structural dynamics studies to provide a comprehensive understanding of system behaviour under seismic loading (ElGawady et al. 2004; Dowling et al. 2014).

4.4 Impact Hammer Testing

An impact hammer test was conducted to determine the natural time period and damping characteristics of all seven models. The experimental setup consisted of an impact hammer, accelerometers, a sixteen-channel vibration analyzer, data acquisition cables, and a computer equipped with NV Gate software.

Each model was first rigidly fixed onto the shake table platform to ensure stability during testing. A concentrated mass of approximately 32 kg was placed on the roof of the model to simulate the effect of roof loading and to achieve realistic dynamic characteristics.

Accelerometers were installed at predefined locations on the model, and all sensors were connected to the vibration analyzer system. After ensuring proper connectivity and calibration, the impact hammer was used to apply a horizontal impulse load to the wall of the model at a selected location.

The impact generated free vibrations in the structure, and the corresponding acceleration–time history was recorded. The natural time period (T) of the structure was determined by measuring the time required to complete one cycle of vibration from the recorded response.

The damping ratio (ξ) was estimated using the logarithmic decrement method based on the decay of peak accelerations: $\varepsilon = \frac{1}{2\pi} \ln\left(\frac{A_1}{A_2}\right)$

Where, A_1 and A_2 represent successive peak accelerations at time t_1 and t_2 respectively.

It is acknowledged that the above formulation strictly applies to systems undergoing uniform exponential decay; however, masonry structures exhibit non-uniform and nonlinear damping characteristics. Therefore, the damping values obtained in this study represent approximate estimates. To improve accuracy, multiple readings were taken, and the results were averaged.

This approach provides a reasonable approximation of damping for comparative evaluation of different models (Chopra 2012).

Table 4. Dynamic characteristics of models obtained from impact hammer testing

Model	Fundamental Natural Time period (T_n)	Damping (ξ)%
U1	0.008	1.54
A1	0.009	2.67
A2	0.01	4.61
B1	0.006	2.24
B2	0.01	2.67
C1	0.01	1.572
C2	0.011	1.551

4.5 Shake Table Testing

The shake table used in this study was a uniaxial servo-controlled system designed for laboratory-scale dynamic testing. The key operational

specifications of the shake table are summarized in Table 4.

Table 5. Specifications of shake table used in the study

Parameter	Details
Table type	Uniaxial shake table
Payload capacity	200 kg
Maximum acceleration	Up to 5g
Frequency range	0–25 Hz
Table size	3 ft × 5 ft
Motor capacity	1 HP

The selected shake table capacity and operational range were adequate for testing reduced-scale adobe masonry models and for simulating dynamic excitation within the frequency range of interest.

Each model was rigidly fixed onto the shake table, and a roof mass of approximately 32 kg was applied to simulate realistic loading conditions. Accelerometers were installed at the base and roof levels of the structure to capture the dynamic response.

The testing procedure involved applying harmonic excitation to the model in a controlled manner. The initial input frequency was set at 1 Hz, with a displacement amplitude of 15 mm and five loading cycles. The frequency was gradually increased in increments, and at each stage, the structural response was recorded.

For each excitation level, the structural response was recorded in terms of base acceleration, roof acceleration, and lateral displacement at the top of the structure. Additionally, input excitation parameters, including frequency, displacement amplitude, and number of loading cycles, were documented for each stage of testing. The collected data were subsequently used for evaluating the seismic response and capacity characteristics of the models.

The data were collected using a sixteen-channel vibration analyzer and stored digitally for further processing.

It is noted that the input frequency of the servo motor may differ slightly from the actual frequency transmitted to the base of the model due to system dynamics. However, for the purpose of comparative analysis, this variation is considered negligible.

The testing was continued until significant damage or complete structural failure was observed. Visual observations of crack initiation, propagation, and collapse mechanisms were recorded throughout the testing process.

The progressive increase in excitation allowed identification of damage thresholds and failure mechanisms for each strengthening configuration, enabling a comparative assessment of seismic performance

5. RESULTS AND DISCUSSION

The seismic performance of the adobe masonry models was evaluated based on dynamic characteristics obtained from impact hammer testing and structural response observed during shake table testing. The results are discussed in terms of natural time period, damping ratio, lateral load capacity, drift behaviour, and failure mechanisms.

5.1. Dynamic Characteristics from Impact Hammer Testing

The natural time period and damping ratio of all models were obtained from impact hammer testing, as summarized in Table 4.

Table 6. Dynamic properties of adobe masonry models obtained from impact hammer testing

Model ID	Strengthening configuration	Natural Time Period (sec)	Damping ratio (%)
U1	Unreinforced	0.008	1.540
A1	Cold-formed steel at corners, openings, and lintel level	0.009	2.670
A2	Cold-formed steel grid reinforcement	0.010	4.610
B1	Geogrid surface strengthening	0.006	2.240
B2	Geogrid bed-joint reinforcement	0.010	2.670
C1	Hemp fibre grid reinforcement	0.010	1.572
C2	Hemp fibre reinforcement at wall junctions	0.011	1.551

The unreinforced model (U1) exhibited a natural time period of 0.008 s and a damping ratio of 1.54%, representing the baseline dynamic response of adobe masonry. The introduction of strengthening systems resulted in noticeable changes in both stiffness and energy dissipation characteristics.

Relative to the unreinforced model, the damping ratio increased by 73.38% in model A1, 199.35% in model A2, 45.45% in model B1, 73.38% in model B2, 2.08% in model C1, and 0.71% in model C2. The most significant increase was observed in model A2, indicating that the cold-formed steel grid configuration is highly effective in enhancing energy dissipation.

The increase in damping in cold-formed steel and geogrid-reinforced models can be attributed to improved frictional interaction, confinement effects, and hysteretic behaviour during vibration. In

contrast, hemp fibre-reinforced models exhibited only marginal improvement in damping due to the relatively flexible nature of the reinforcement.

In terms of stiffness, the geogrid surface-reinforced model (B1) exhibited the lowest time period (0.006 sec), indicating the highest stiffness among all configurations. It is noteworthy that models A2, B2, and C2 exhibited higher natural time periods compared to the unreinforced model, indicating increased flexibility due to the distribution and nature of reinforcement. The reduction in time period in strengthened models reflects improved structural rigidity due to confinement and tensile reinforcement mechanisms.

5.2 Seismic Response under Shake Table Testing

Shake table testing was conducted to evaluate the response of the models under progressively increasing dynamic excitation. The structural behaviour of the models is presented in terms of base shear coefficient versus drift ratio, as shown in Fig. XX.

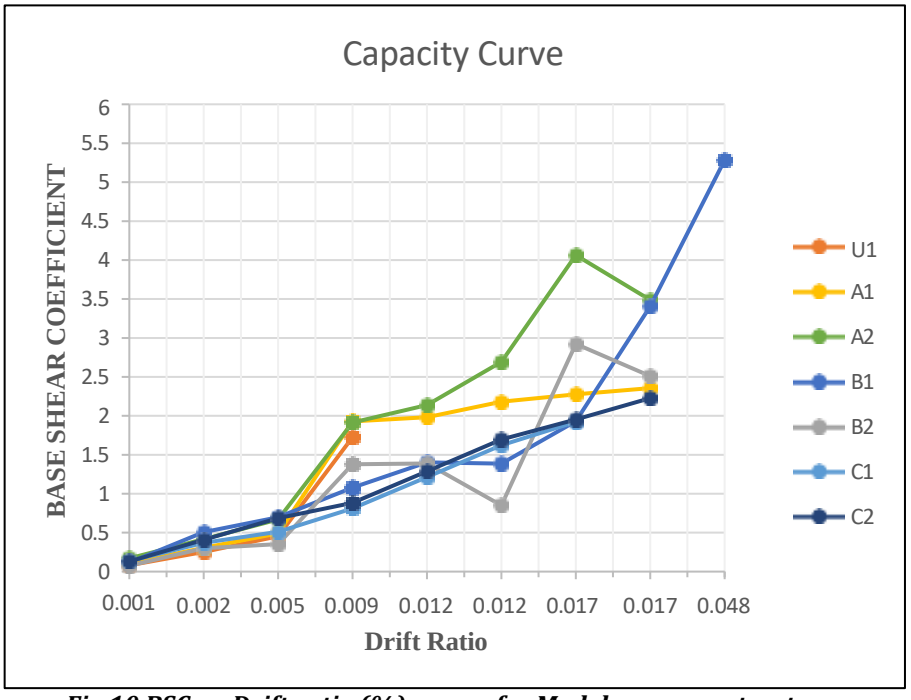

Fig 10 BSC vs. Drift ratio (%) curves for Model masonry structures

The unreinforced model (U1) exhibited brittle behaviour, characterized by early crack initiation and sudden failure at relatively low drift levels. In contrast, all strengthened models demonstrated improved performance, with delayed crack initiation, increased load-carrying capacity, and enhanced deformation capacity.

The strengthened models exhibited delayed crack initiation, higher base shear resistance, and increased drift capacity, indicating improved post-elastic behaviour compared to the unreinforced model.

5.3 Load–Deformation Behaviour

The capacity curves indicate that strengthening techniques significantly influence the load–deformation behaviour of adobe masonry structures. The geogrid surface-reinforced model (B1) exhibited the highest base shear capacity, which can be attributed to effective confinement and improved stress distribution within the masonry. The maximum base shear capacity of model B1 was approximately 150–180% higher than that of the unreinforced model, confirming the effectiveness of confinement-based strengthening

The cold-formed steel grid model (A2) also demonstrated substantial strength enhancement due to distributed tensile reinforcement.

Models reinforced with hemp fibre (C1 and C2) showed comparatively lower strength enhancement but exhibited improved deformation characteristics, indicating enhanced ductility.

5.4 Drift Capacity and Ductility

The drift ratio at failure is a key indicator of structural ductility. The unreinforced model failed at relatively low drift levels, confirming its brittle nature.

Strengthened models exhibited higher drift capacities, indicating improved deformation capability. Among the tested configurations, hemp fibre-reinforced models (C1 and C2) exhibited higher drift capacity due to their flexible reinforcement

mechanism, whereas geogrid-reinforced models provided a balanced improvement in both strength and ductility. Cold-formed steel reinforcement increased stiffness but resulted in comparatively lower deformation capacity.

These observations highlight the trade-off between stiffness and ductility in different strengthening techniques.

5.5 Failure Mechanisms and Crack Patterns

The failure patterns observed during shake table testing are presented in Fig. 14-24.

Fig 11 Model U1 On Shake Table

Fig 12 Model A1 On Shake Table

Fig 13 Model A2 On Shake Table

Fig 14 Collapse of Model U1

Fig 15 Collapse of Model A1

Fig 16 Collapse of Model A2

Fig 17 Model B1 On Shake Table

Fig 18 Model B2 On Shake Table

Fig 19 Collapse of Model B1

Fig 20 Collapse of Model B2

Fig 21 Model C1 On Shake Table

Fig 22 Model C2 On Shake Table

Fig 23 Collaose of Model C1

Fig 24 Collapse of Model C2

The unreinforced model exhibited diagonal shear cracking originating near openings and propagating towards wall corners, ultimately leading to sudden and brittle collapse. In contrast, strengthened models demonstrated distributed cracking patterns with delayed crack propagation, indicating improved stress redistribution and structural integrity.

Cold-formed steel reinforcement effectively limited crack widths and prevented abrupt failure. Geogrid reinforcement provided confinement, resulting in distributed cracking and improved load transfer. Hemp fibre reinforcement acted as a crack-bridging mechanism, enabling controlled deformation and preventing sudden collapse.

5.6 Comparative Performance of Strengthening Techniques

A comparative evaluation of the strengthening techniques indicates that geogrid surface reinforcement (B1) is the most effective in enhancing stiffness and lateral load capacity due to its confinement action. Cold-formed steel grid reinforcement (A2) provides the highest energy dissipation capacity, as reflected by the significant increase in damping ratio. Hemp fibre reinforcement (C1 and C2), although less effective in increasing strength, contributes to improved ductility and deformation capacity through crack-bridging mechanisms. These results demonstrate that the selection of strengthening technique should be based on the desired performance objective, whether stiffness, strength, or ductility

5.7 Discussion on Structural Implications

The experimental results highlight that the effectiveness of strengthening techniques is governed by their reinforcement mechanism. Confinement-based systems, such as geogrid reinforcement, enhance lateral load capacity by improving stress redistribution and delaying crack propagation. Tensile reinforcement systems, such as cold-formed steel, contribute significantly to energy dissipation through hysteretic behaviour. Fibre-based systems, such as hemp reinforcement, improve deformation capacity and mitigate brittle failure by enabling crack bridging. These findings are consistent with previous experimental studies on reinforced masonry systems (Tipler et al. 2010; Ye et al. 2018; Behera et al. 2022).

Overall, the results demonstrate that appropriate strengthening strategies can transform the inherently brittle behaviour of adobe masonry into a more ductile and energy-dissipative structural system under seismic loading.

6. CONCLUSIONS

This study presented a systematic experimental investigation on the seismic performance of adobe masonry structures strengthened using cold-formed steel, geogrid, and hemp fibre reinforcement systems. Reduced-scale models were tested under identical conditions using impact hammer and shake table testing to enable direct comparison of strengthening mechanisms. Based on the experimental observations and analysis, the following conclusions are drawn:

(1) Modification of dynamic characteristics

The incorporation of strengthening systems significantly influenced the dynamic properties of adobe masonry. Cold-formed steel grid reinforcement (A2) resulted in the highest increase in damping ratio, indicating enhanced energy dissipation through hysteretic behaviour. Geogrid surface reinforcement (B1) exhibited the lowest natural time period, reflecting increased stiffness due to effective confinement. However, certain configurations (A2, B2, and C2) showed relatively higher time periods, suggesting that reinforcement distribution and interaction with the adobe matrix may introduce localized flexibility.

(2) Enhancement of seismic load-carrying capacity

All strengthening systems improved the seismic resistance of adobe masonry compared to the unreinforced model. Among them, geogrid surface reinforcement (B1) demonstrated the highest base shear capacity, confirming the effectiveness of confinement-based strengthening in enhancing load

transfer and delaying structural degradation.

(3) Influence on ductility and deformation behaviour

Hemp fibre reinforcement (C1 and C2) was found to significantly improve deformation capacity and ductility. The flexible nature of the fibre system enabled crack bridging and controlled deformation, thereby reducing the tendency for brittle failure. However, its contribution to strength enhancement remained limited compared to metallic and geosynthetic systems.

(4) Behaviour of cold-formed steel reinforcement

Cold-formed steel reinforcement improved crack control and energy dissipation characteristics, particularly in the grid configuration (A2). Nevertheless, the effectiveness of steel reinforcement was influenced by its bond interaction with the adobe matrix, and failure was governed primarily by the masonry rather than the reinforcement itself.

(5) Modification of failure mechanisms

The unreinforced model exhibited brittle failure characterized by diagonal cracking and sudden collapse. In contrast, strengthened models showed delayed crack initiation, distributed cracking patterns, and improved structural integrity. The strengthening systems effectively altered the failure mechanism from brittle to more controlled and ductile behaviour.

(6) Comparative effectiveness of strengthening systems

The study highlights that the performance of strengthening techniques is governed by their reinforcement mechanism:

Geogrid reinforcement provides superior stiffness and load-carrying capacity through confinement effects.

Cold-formed steel reinforcement enhances energy dissipation and crack control.

Hemp fibre reinforcement improves ductility and deformation capacity through flexible load transfer and crack-bridging behaviour.

(7) Practical implications for seismic strengthening

The results demonstrate that low-cost and locally adaptable strengthening techniques can significantly enhance the seismic resilience of adobe masonry structures. Geogrid and hemp fibre systems offer practical and sustainable solutions for application in rural and resource-limited regions, while cold-formed steel systems provide improved performance where higher structural reliability is required.

6.1 Limitations of the Study

Despite the valuable insights obtained from the experimental investigation, certain limitations should be acknowledged. The study was conducted on reduced-scale models, and therefore, scaling effects may influence the absolute dynamic response of the structures. In addition, the shake table testing was performed using controlled harmonic excitation, which may not fully replicate the complexity of real earthquake ground motions. Furthermore, the inherent variability associated with adobe materials was not extensively investigated, and the properties used in the study represent a specific material composition. The interaction between reinforcement systems and the adobe matrix, particularly the bond behaviour, was also not explicitly quantified. These limitations should be considered when extrapolating the results to full-scale structures and real-world applications.

6.2 Recommendations for Future Research

Further research is required to extend and validate the findings of the present study. Future investigations should focus on the behaviour of full-scale adobe masonry structures subjected to realistic earthquake ground motions in order to better capture actual seismic response. The long-term durability and environmental performance of strengthening materials, particularly natural fibre systems, should also be evaluated under varying climatic conditions. In addition, detailed experimental and numerical studies are needed to quantify the bond interaction between reinforcement systems and adobe masonry, which plays a critical role in structural performance. The development and validation of numerical models based on the experimental results would enable predictive analysis and design optimization. Finally, there is a need to formulate practical design guidelines for the implementation of these strengthening techniques in real-world applications, particularly in resource-constrained and seismically vulnerable regions.

REFERENCES

1. Adhikari, R., et al. (2023). “Seismic performance assessment of masonry buildings.” Buildings, 13(5).
2. Akhoundi, F., et al. (2024). “Seismic behaviour of confined masonry structures under dynamic loading.” Structures.

3. Arya, A. S., Boen, T., and Ishiyama, Y. (2013). Guidelines for earthquake resistant non-engineered construction. IAEE.
4. Banerjee, S., et al. (2021). "Seismic performance of confined masonry structures." Engineering Structures, 242.
5. Bothara, J., and Brzev, S. (2011). Improving the seismic performance of stone masonry buildings. EERI, Oakland.
6. Calderini, C., and Lagomarsino, S. (2022). "Experimental and numerical analysis of masonry buildings subjected to earthquake loading." Engineering Structures, 261.
7. Degli Abbati, S., et al. (2023). "Shake table testing of masonry building aggregates." Earthquake Engineering and Structural Dynamics.
8. Dowling, D., Samali, B., and Li, J. (2014). "Experimental study on the dynamic behaviour of mud-brick structures." Journal of Structural Engineering, 140(5).
9. ElGawady, M. A., Lestuzzi, P., and Badoux, M. (2004). "Shake table testing of masonry structures." Earthquake Engineering and Structural Dynamics, 33(7), 857–879.
10. FEMA 306. (1998). Evaluation of earthquake damaged concrete and masonry wall buildings. FEMA, Washington, DC.
11. Griffith, M. C., Vaculik, J., and Lam, N. (2003). "Seismic behaviour of unreinforced masonry structures." Earthquake Engineering and Structural Dynamics, 32.
12. Ikuga, L. M., and Murray, T. (2012). "Vernacular housing." Encyclopedia of Housing, Elsevier.
13. IS 13828. (1993). Improving earthquake resistance of low-strength masonry buildings. BIS, New Delhi.
14. IS 1893 (Part 1). (2016). Criteria for earthquake resistant design of structures. BIS, New Delhi.
15. IS 4326. (1993). Earthquake resistant design and construction of buildings. BIS, New Delhi.
16. IS 2185 (Part 1). (2005). Concrete masonry units—Specification. BIS, New Delhi.
17. Kafodya, I., Okonta, F., and Kloukinas, P. (2019). "Role of fiber inclusion in adobe masonry construction." Journal of Building Engineering, 23.
18. Kaya, A., et al. (2024). "Shake table experimental investigation of masonry structures." Meccanica.
19. Lagomarsino, S., and Giovinazzi, S. (2006). "Macroseismic and mechanical models for vulnerability assessment of masonry buildings." Earthquake Spectra, 22(2), 445–463.
20. Lourenço, P. B. (2006). "Computational strategies for masonry structures." Computers and Structures, 84(31–32), 1977–1988.
21. Minke, G. (2006). Building with earth: Design and technology of a sustainable architecture. Birkhäuser.
22. NZS 4298. (1998). Materials and workmanship for earth buildings. Standards New Zealand.
23. Paulay, T., and Priestley, M. J. N. (1992). Seismic design of reinforced concrete and masonry buildings. Wiley, New York.
24. Reyes, J. C., et al. (2012). "Seismic retrofitting of existing earthen structures using steel plates." Materials and Structures.
25. Samali, B., Dowling, D. M., and Li, J. (2017). "Dynamic testing and analysis of adobe-mudbrick structures." Australian Journal of Structural Engineering.
26. Samali, B., Jinwuth, W., Heathcote, K., and Wang, C. (2011). "Seismic capacity comparison between square and circular plan adobe construction." Procedia Engineering, 14, 2103–2108.
27. Silveira, D., Varum, H., and Costa, A. (2012). "Influence of testing procedures on the mechanical characterization of adobe bricks." Construction and Building Materials, 30, 408–416.
28. Silveira, D., Varum, H., Costa, A., et al. (2012). "Seismic behavior of adobe buildings." Engineering Structures.
29. Tipler, J. F., Worth, M. L., Morris, H. W., and Ma, Q. T. (2010). "Shake table testing of geogrid-reinforced adobe wall models." NZSEE Conference.
30. Tolles, E. L., and Krawinkler, H. (1990). "Seismic studies on small-scale models on adobe houses." Report No. 91, NSF.
31. Tomazevic, M. (1999). Earthquake-resistant design of masonry buildings. Imperial College Press.
32. Ye, J., Becque, J., Hajirasouliha, I., Mojtabaei, S. M., and Lim, J. B. P. (2018). "Development of optimum cold-formed steel sections for maximum energy dissipation." Engineering Structures, 168.